Analysis of Galloping Amplitude for Conductors With Inter-phase Spacers

Hwan-Seong Kim† **and Tuong-Long Nguyen***

Abstract - The main purpose of this paper is to calculate the behaviors of inter-phase spacers to reduce the amplitude of galloping in conductors. In simulation, three phases and iced-single/two-bundles conductors with/without spacers are considered in viewpoint of standard cases. The implicit/explicit finite element methods are used to calculate the transient response with geometric nonlinear behavior. The ANSYS/LS-DYNA program is also applied. Calculation results can be used to predict the positions to insert the inter-phase spacers between conductors.

Keywords: Geometric Nonlinear Behavior, Inter-phase Spacers, Power Transmission Lines

1. Introduction

Galloping, which is defined as the instability of aerodynamic and aero elasticity on overhead line conductors, is the typical phenomenon of slender structures. Since the early 1920's, galloping of iced conductors has posed a design and operating problem, especially in the case of overhead power transmission line conductors with low frequency (from 0.15 [Hz] to 1 [Hz]) and high amplitude galloping [1-2]. For understanding the mechanisms and finding out the solution of galloping problems, various models have been developed as simulations [3-6]. There are two kinds of simulations, one based on the experiment with real test conducted lines and the other with numerical computing. In numerical simulation, two cases of linear/non-linear differential equations and finite element modeling method were used.

In practical simulation, to avoid the galloping, some mechanical devices such as the pendulum detuner, windamper, twister, torsional damper detuner, inter-phase spacers, etc., were applied. In the case of using inter-phase spacers, the problem is that it will affect the vibration of the power transmission line (PTL). Conversely, when the iced conductors are subjected to wind flow; its vibration may increase or its motion may suddenly deflect. Thus, it causes the cables from two different phases to come too close to each other, and consequently repeated short-circuiting is created.

Recently, simulation methods based on quasi-steady theory of the aerodynamic loading for galloping have been studied [7-8]. In these results, lift, drag and torque coefficient may be formerly measured in the wind tunnel as a function of wind angle.

The main purpose of this paper is to calculate the behaviors of inter-phase spacers to reduce the amplitude of galloping in conductors.

In simulation, three phases and iced single two bundle conductors with and without spacers are considered in the viewpoint of standard cases. The implicit and explicit finite element methods are used to calculate the transient response with geometric nonlinear behavior. The ANSYS/LS DYNA program is also applied [9-12]. Calculation results can be used to predict the positions to insert the inter-phase spacers between conductors.

2. General Analysis Procedure

In this procedure, the power transmission lines are modeled by beam elements that undergo very large displacements. The element description is based on a rigid convected co-ordinate or co-rotational formulation described by Belytschko [10-12].

Moreover, the formulation is intended for explicit temporal integration procedures, so stiffness matrices are not developed.

2.1 Co-ordinate Systems

The element coordinate system is defined to have the local x-axis $\hat{x}$ originating at node I and terminating at node J, the local y-axis $\hat{y}$ and the local z-axis $\hat{z}$.

The element coordinate system($x, y, \hat{z}$) and associated

† Corresponding Author: Dept. of Logistics, Korea Maritime University, Korea (kimhs@mail.hhu.ac.kr)
* Dept. of Engineering Mechanics, Faculty of Applied Science, Hochiminh City University of Technology, VietNam (ntlong@hcmut.edu.vn)
Received December 24, 2004 ; Accepted August 3, 2005

unit vector triad (e_1, e_2, e_3) are updated at every time step by the same technique used to construct the initial system as in Fig. 1.

The unit vectors of the two coordinate systems define rotational transformations between the global coordinate system and each respective coordinate system.

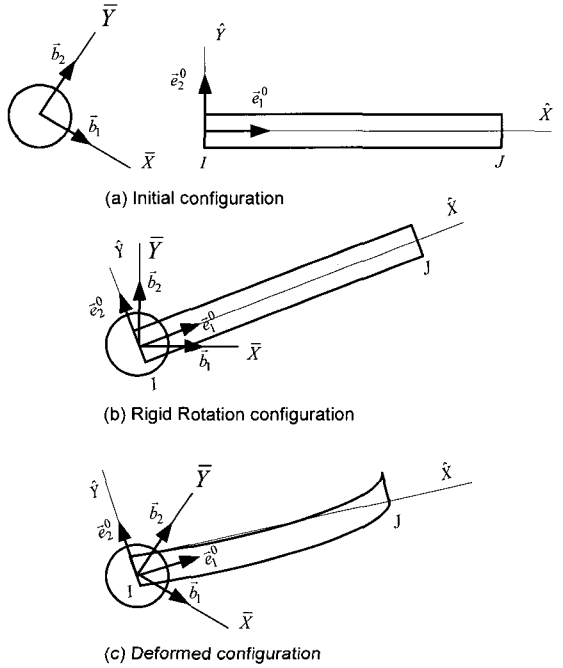

Fig. 1 Co-rotational coordinate system

These transformations operate on vectors with global component A, body coordinate component $\bar{A}$, and element coordinate component $\hat{A}$, which are defined as.

$$A = \begin{Bmatrix} A_x \\ A_y \\ A_z \end{Bmatrix} = \begin{bmatrix} b_{1x} & b_{2x} & b_{3x} \\ b_{1y} & b_{2y} & b_{3y} \\ b_{1z} & b_{2z} & b_{3z} \end{bmatrix} \begin{Bmatrix} \bar{A}_x \\ \bar{A}_y \\ \bar{A}_z \end{Bmatrix} = [\lambda]\{\bar{A}\} \tag{1}$$

where b_{ix}, b_{iy}, b_{iz} denote the global components of the body coordinate unit vectors. Similarly, the element coordinate system is defined as

$$A = \begin{Bmatrix} A_x \\ A_y \\ A_z \end{Bmatrix} = \begin{bmatrix} e_{1x} & e_{2x} & e_{3x} \\ e_{1y} & e_{2y} & e_{3y} \\ e_{1z} & e_{2z} & e_{3z} \end{bmatrix} \begin{Bmatrix} \hat{A}_x \\ \hat{A}_y \\ \hat{A}_z \end{Bmatrix} = [\mu]\{\hat{A}\} \tag{2}$$

where e_{ix}, e_{iy}, e_{iz} denote the global components of the element coordinate unit vectors. The inverse transformation is defined by the matrix transpose, i.e.

$$\{\bar{A}\} = [\lambda]^T \{A\} \tag{3}$$

$$\{\hat{A}\} = [\mu]^T \{A\} \tag{4}$$

2.2 Equations of Motion

The translation equations of motion are given on node I.

$$\rho_I \ddot{u}_{iI} = F_{iI}^{ext} - F_{iI}^{int} \tag{5}$$

where ρ_I denotes the translational inertia of node I.

The rotational equations are the usual Euler equations of rigid body dynamics, on node I.

$$\begin{aligned} I_{xxI}\alpha_{xI} + (I_{zzI} - I_{yyI})\omega_{yI}\omega_{zI} &= M_{xI}^{ext} - M_{xI}^{int} \\ I_{yyI}\alpha_{yI} + (I_{xxI} - I_{zzI})\omega_{xI}\omega_{zI} &= M_{yI}^{ext} - M_{yI}^{int} \\ I_{zzI}\alpha_{zI} + (I_{yyI} - I_{xxI})\omega_{xI}\omega_{yI} &= M_{zI}^{ext} - M_{zI}^{int} \end{aligned} \tag{6}$$

where I_{xx}, I_{yy} and I_{zz} denote the principal moments of inertia.

The displacements of the element are decomposed into rigid body displacements r_i and deformation displacements d_i.

$$u_i = r_i + d_i \tag{7}$$

The strains are given by

$$\hat{\varepsilon}_{ij} = \frac{1}{2}\left(\frac{\partial \hat{d}_i}{\partial \hat{x}_j} + \frac{\partial \hat{d}_j}{\partial \hat{x}_i} \right) \tag{8}$$

which can be expressed for an element in matrix form

$$\{\hat{\varepsilon}\} = [E]\{\hat{d}\} \tag{9}$$

where $\{\hat{d}\}$ denotes the matrix of nodal deformation displacements.

And

$$\{\hat{d}\} = [T]\{u\} \tag{10}$$

The nodal element forces $\{f^{\text{int}}\}$ are given by

$$\{\hat{d}\} = [T]\{u\} \tag{11}$$

$$\left\{f^d\right\} = \int_V [E]^T \{\hat{\sigma}\} dV \tag{12}$$

where V denotes the volume of the element, $\{\hat{\sigma}\}$ the stresses measured in the rotated co-ordinates $\{\hat{x}_i\}$, and $\left\{f^d\right\}$ the nodal forces conjugate to $\{d\}$.

$$\{d\}^T \left\{f^d\right\} = w^{\text{int}} \tag{13}$$

where $\left\{w^{\text{int}}\right\}$ denotes the internal work.

2.3 Belytschko Beam Element Formulation

The deformation displacements are given by

$$\hat{d}^T = \left\{\delta_{IJ}, \hat{\theta}_{xJI}, \hat{\theta}_{yI}, \hat{\theta}_{yJ}, \hat{\theta}_{zI}, \hat{\theta}_{zJ}\right\} \tag{14}$$

where δ_{IJ}, $\hat{\theta}_{xJI}$ denote length change, torsional deformation, and $\hat{\theta}_{yI}$, $\hat{\theta}_{yJ}$, $\hat{\theta}_{zI}$, $\hat{\theta}_{zJ}$ denote bending rotational deformations.

The superscript ^ denotes that theses quantities are defined in the local element coordinate system, and I and J are the nodes at the ends of the beam.

The deformation displacements are given by the elongation of the beam is calculated directly from the original nodal coordinates (X_I, Y_I, Z_I) and the total displacements (u_{xI}, u_{yI}, u_{zI})

$$\delta_{IJ} = \frac{[2(X_{JI}u_{xJI} + X_{JI}u_{yJI} + Z_{JI}u_{zJI}) + u_{xJI}^2]}{l + l^0} + \frac{\left[+u_{xJI}^2 + u_{yJI}^2 + u_{zJI}^2\right]}{l + l^0} \tag{15}$$

where

$$X_{JI} = X_J - X_I$$
$$u_{xJI} = u_{xJ} - u_{xI}; \quad etc.$$

For the purpose of computing the relative rotations, $\hat{\theta}_{yI}, \hat{\theta}_{zI}, \hat{\theta}_{yJ}, \hat{\theta}_{zJ}$, and $\hat{\theta}_{xJI}$, the body components of the unit vectors e_1^o and e_2^o must be stored for each of the two nodes of the element.

$$\hat{\theta}_y e_2 + \hat{\theta}_z e_3 = \det\begin{bmatrix} e_1 & e_2 & e_3 \\ 1 & 0 & 0 \\ \hat{e}_{1x}^0 & \hat{e}_{1y}^0 & \hat{e}_{1z}^0 \end{bmatrix} = -\hat{e}_{1z}^0 e_2 + \hat{e}_{1y}^0 e_3 \tag{16}$$

Then

$$\hat{\theta}_y = -\hat{e}_{1z}^0 ; \qquad \hat{\theta}_z = \hat{e}_{1y}^0 \tag{17}$$

$$\hat{\theta}_{xIJ} = e_1.(e_{2I}^0 \times e_{2J}^0) = e_1 \det\begin{bmatrix} e_1 & e_2 & e_3 \\ \hat{e}_{x2I}^0 & \hat{e}_{y2I}^0 & \hat{e}_{z2I}^0 \\ \hat{e}_{x2J}^0 & \hat{e}_{y2J}^0 & \hat{e}_{z2J}^0 \end{bmatrix} = \hat{e}_{y2I}^0 \hat{e}_{z2J}^0 - \hat{e}_{y2J}^0 \hat{e}_{z2I}^0 \tag{18}$$

Eqs. (15), (17) and (18) require the assumption that the deformation displacement of an element is small.

2.4 The Shape Functions

The deformation displacement field for the beam element is considered to consist of transverse displacements that are cubic functions of $\hat{x}$.

And, the axial displacement is a linear function of $\hat{x}$.

$$\hat{d}_x^m = (1-\xi)\hat{d}_{xI} + \xi \hat{d}_{xJ} \tag{19}$$

$$\hat{d}_y^m = (\xi - 2\xi^2 + \xi^3) l \hat{\theta}_{zI} + (-\xi^2 + \xi^3) l \hat{\theta}_{zJ} \tag{20}$$

$$\hat{d}_z^m = (-\xi + 2\xi^2 - \xi^3) l \hat{\theta}_{yI} + (\xi^2 - \xi^3) l \hat{\theta}_{yJ} \tag{21}$$

$$\hat{\theta}_x = \xi \hat{\theta}_{xJI} \tag{22}$$

where

$$\xi = \frac{\hat{x}}{l}$$

And $\hat{x}$ is taken to originate at node I. Superscript m is used to indicate that these are the displacement of the mid surface.

2.5 Bending Moments

The bending moments are related to the deformation rotations by

$$\begin{Bmatrix} \hat{m}_{yI} \\ \hat{m}_{yJ} \end{Bmatrix} = \frac{K_y^b}{1+\phi_y} \begin{bmatrix} 4+\phi_y & 2-\phi_y \\ 2-\phi_y & 4+\phi_y \end{bmatrix} \begin{Bmatrix} \hat{\theta}_{yI} \\ \hat{\theta}_{yJ} \end{Bmatrix} \tag{23}$$

$$\begin{Bmatrix} \hat{m}_{zI} \\ \hat{m}_{zJ} \end{Bmatrix} = \frac{K_z^b}{1+\phi_z} \begin{bmatrix} 4+\phi_z & 2-\phi_z \\ 2-\phi_z & 4+\phi_z \end{bmatrix} \begin{Bmatrix} \hat{\theta}_{zI} \\ \hat{\theta}_{zJ} \end{Bmatrix} \tag{24}$$

The bending constants are given by

$$K_y^b = \frac{EI_{yy}}{l^0}, \text{ and } \quad K_z^b = \frac{EI_{zz}}{l^0} \tag{25}$$

$$I_{yy} = \iint \hat{z}^2 d\hat{y} d\hat{z} \tag{26}$$

$$I_{zz} = \iint \hat{y}^2 d\hat{y} d\hat{z} \tag{27}$$

$$\phi_y = \frac{12EI_{yy}}{GA_s l^2} \tag{28}$$

$$\phi_z = \frac{12EI_{zz}}{GA_s l^2} \tag{29}$$

Hence ϕ, G and A_s denote the shear factor, the shear modulus and the effective area in shear, respectively.

2.6 Torsional Moment

The torsional moment is calculated from the torsional deformation rotation as

$$\hat{m}_{xJ} = K^t \hat{\theta}_{xJI} \tag{30}$$

where

$$K^t = \frac{GJ}{l^0} \quad \text{and} \quad J = \iint \hat{y}\hat{z} d\hat{y} d\hat{z}$$

2.7 Temporal Integration

The equations of motion are integrated by the Newmark β - method with $\beta = 0$, which is almost identical to the central difference method.

These formulas predict the velocities and displacements at the end of the time step. The translational components are given by

$$\dot{u}_{iI}^{j+1} = \dot{u}_{iI}^{j} + \frac{1}{2}\Delta t(\ddot{u}_{iI}^{j} + \ddot{u}_{iI}^{j+1}) \tag{31}$$

$$u_{iI}^{j+1} = u_{iI}^{j} + \Delta t \dot{u}_{iI}^{j} + \frac{1}{2}\Delta t^2 \ddot{u}_{iI}^{j} \tag{32}$$

where the superscripts denote the time step and Δt is the time increment during a step.

In particular, the body component unit vectors are updated using the formula

$$b_i^{j+1} = b_i^j + \Delta t \frac{db_i^j}{dt} + \frac{\Delta t^2}{2} \frac{d^2 b_i^j}{dt^2} \tag{33}$$

The time derivatives in the above equation (33) are replaced by their equivalent forms from vector analysis

$$\frac{db_i}{dt} = \omega \cdot b_i \tag{34}$$

$$\frac{d^2 b_i}{dt^2} = \omega \times (\omega \times b_i) + (\alpha \times b_i) \tag{35}$$

where ω and α denote vectors of angular velocity and acceleration, respectively. With the above relations substituted into Eq. (33), the updated formula for the unit vectors becomes

$$\begin{aligned} b_i^{j+1} &= b_i^j + \Delta t(\omega \cdot b_i^j) + \\ &\frac{1}{2}\Delta t^2[\omega \times (\omega \times b_i^j) + (\alpha \times b_i^j)] \end{aligned} \tag{36}$$

The updated $\bar{x}$ component of b_3 is found by letting $i = 3$ in equation (36) and taking the scalar product of both sides of the equation with b_1, which yields, after some simplification

$$\begin{aligned} \bar{b}_{x3}^{j+1} &= b_1^j \cdot b_3^{j+1} \\ &= \Delta t \omega_y^j + \frac{1}{2}\Delta t^2(\omega_x^j \omega_z^j + \alpha_y^j) \end{aligned} \tag{37}$$

Similarly

$$\begin{aligned} \bar{b}_{y3}^{j+1} &= b_2^j \cdot b_3^{j+1} \\ &= -\Delta t \omega_x^j + \frac{1}{2}\Delta t^2(\omega_y^j \omega_z^j - \alpha_x^j) \end{aligned} \tag{38}$$

$$\bar{b}_{y1}^{j+1} = b_1^j \cdot b_2^{j+1} = \Delta t \omega_z^j + \frac{1}{2}\Delta t^2(\omega_x^j \omega_y^j - \alpha_z^j) \tag{39}$$

Since b_3^{j+1} is a unit vector, normality provides the relation

$$\bar{b}_{z3}^{j+1} = \sqrt{1-\left(\bar{b}_{x3}^{j+1}\right)^2 - \left(\bar{b}_{y3}^{j+1}\right)^2} \tag{40}$$

It is assumed that $b_{x1}^{j+1} \approx 1$, orthogonality yields

$$\bar{b}_{z1}^{j+1} = -\frac{\bar{b}_{x3}^{j+1} + \bar{b}_{y1}^{j+1}\bar{b}_{y3}^{j+1}}{\bar{b}_{z3}^{j+1}} \tag{41}$$

The component $\bar{b}_{x1}^{j+1}$ is then found by enforcing normality

$$\bar{b}_{x1}^{j+1} = \sqrt{1-\left(\bar{b}_{y1}^{j+1}\right)^2 - \left(\bar{b}_{z1}^{j+1}\right)^2} \tag{42}$$

The update components of b_1 and b_3 are defined relative to the body coordinates at time step j. Using Eq. (3) with λ defined at step j, and their vector cross product is used to form b_2.

2.8 Using ANSYS/ LS-DYNA Program

The deformation displacement field for the beam element is considered to consist of transverse displacements that are cubic functions of $\hat{x}$.

A modal analysis of the structure should be initially performed to provide information about the structure's dynamic behavior. Then, the explicit finite element method is used to determine the displacement response of galloping for power transmission lines.

2.8.1 Modal Analysis

The first step in a modal analysis is to extract a set of response modes. These can be obtained by performing an implicit eigenvalue analysis. After computing the stiffness and mass matrices K and M, the following system is constructed

$$(K - \omega^2 M)\phi = 0 \tag{43}$$

and solved for the eigenvalue ω^2 and corresponding eigenvectors (mode shapes) ϕ_i.

The basic algorithm of the block Lanczos method [13] is used to determine the natural frequency of models. This method uses the sparse matrix solver. Beam 4 element is applied for models.

2.8.2 Transient Dynamic Analysis

The explicit finite element method is shown in Table 1, with the approximations of small rotations implicit in Eqs. 41-42.

We also applied an ALPHA damping coefficient equal to 0.019 to all materials. ANSYS/ LS-DYNA automatically converts the implicit Beam 4 elements to explicit Beam161 elements.

Table 1 The Flow chart for computational procedure

	Flow chart
(1)	Set initial conditions, $t = 0$
(2)	Update displacement, $\{u(t+\Delta t)\}$ by Eq. (32)
(3)	Update unit vectors b_1 by Eqs. (37)-(42) and transform to global components by Eq. (3). Loop on number of elements.
(4)	Find deformation displacement $\{d\}$ by Eqs. (15), (16) and (18).
(5)	Find the strain in the convected co-ordinates, $\{\hat{\varepsilon}\}$ by Eq. (8).
(6)	Stress-strain law
(7)	Find local nodal forces $\{f^d\}$ by Eq. (12), transform to $\{f^{\text{int}}\}$
(8)	Add $\{f^{\text{int}}\}$ into $\{F^{\text{int}}\}$. End of loop
(9)	Compute $\{\ddot{u}(t+\Delta t)\}$ by Eq. (5), and $\{\alpha(t+\Delta t)\}$ by Eq. (6).
(10)	Compute $\{\dot{u}(t+\Delta t)\}$ by Eq. (31), and $\{\omega(t+\Delta t)\}$ by Eq. (31)
(11)	$t \leftarrow t+\Delta t$, go to (2)

3. Modeling Considerations

In this paper, we assume the following 154 kV overhead power transmission line with inter-phase spacer

(hanging composite polymer spacer) in Fig. 2.

In a $154\,kV$ overhead power transmission line, generally an aluminum conductor steel reinforced (ACSR) type is used [14].

The ACSR electrical conductor (with 26 aluminum wires and 7 steel wires) was used throughout this paper. The tower sketch is used by the standard phase to phase distance ($3.8\,[m]$ and $4.3\,[m]$).

A span of conductor with ends at the same altitude is shown in the following equation

$$y = \frac{H}{m}\left[\cosh\left(\frac{m}{H}x\right) - 1\right] \tag{44}$$

The parameters of the model are presented in Table 2. The model of a non circular cross section is given below in Fig. 3.

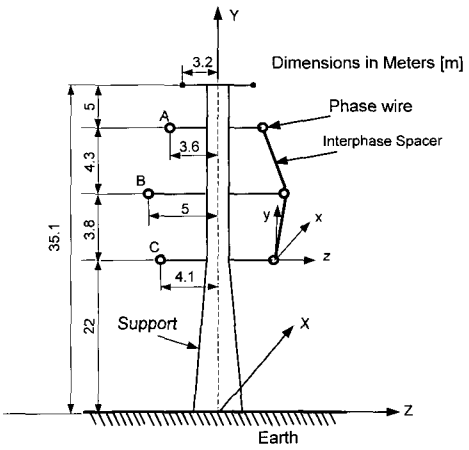

Fig. 2 Characteristics of PTL and spacers.

Table 2 Model parameters

	Symbols	Values	Units
(1)	Traveling wave velocity	131.3	$[m/s]$
(2)	Horizontal tension	44455	$[N]$
(3)	Span	250	$[m]$
(4)	Mass of ice	0.128	$[kg/m]$
(5)	Mass of conductor	1.673	$[kg/m]$
(6)	Young's modulus of conductor	$8.93e^{10}$	$[N/m^2]$
(7)	Density of conductor	3480	$[kg/m^3]$
(8)	Young's modulus of ice	$14.9e^{3}$	$[N/m^2]$
(9)	Density of ice	917	$[kg/m^3]$
(10)	Young's modulus of spacer	$41e^{9}$	$[N/m^2]$
(11)	Density of spacer	2021	$[kg/m^3]$

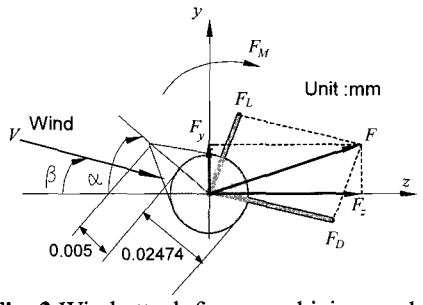

Fig. 3 Wind attack forces and icing angle.

Fig. 3 denotes the definitions of the forces and shows the relation between wind forces, lift and drag forces, where, α denotes icing angle, β is angle of wind attack, V denotes a wind velocity, F_L and F_D represent lift force and drag force, respectively.

These forces F_L, F_D and movement F_M are given as

$$F_D = \frac{1}{2}C_D\rho V^2 s \tag{45}$$

$$F_L = \frac{1}{2}C_L\rho V^2 s \tag{46}$$

$$F_M = \frac{1}{2}C_M\rho V^2 s D_{IC} \tag{47}$$

where, C_L is coefficient of lift force, C_D is coefficient of drag force, ρ is mass density of air, D_{IC} is diameter of ice conductor, and s is area acting wind force.

By considering the angle of wind attack, the forces on y and z axes are given as

$$F_z = F_D\cos\beta + F_L\sin\beta \tag{48}$$

$$F_y = F_L\cos\beta + F_D\sin\beta \tag{49}$$

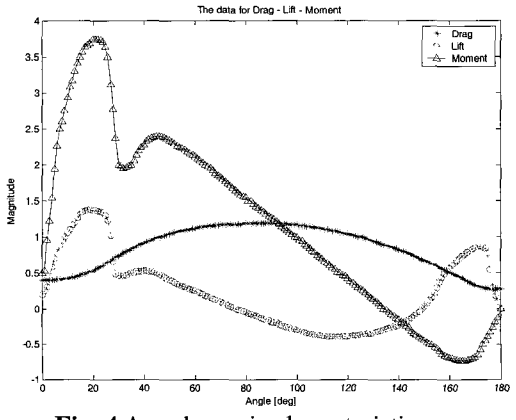

Fig. 4 Aerodynamic characteristics.

Generally, the lift and drag forces depends on the icing shape, ice size, and icing angle etc. For galloping simulation, the data for lift, drag forces and moment are necessary. In this paper, we use the results in [3], which were obtained by wind tunnel test as in Fig. 4.

4. Analysis Results

In analysis results, three phases and iced-single two bundle conductors with and without spacers are considered in 5 cases as in Fig. 5-7.

Beam 161-element is applied for the ice-conductor. It is defined by two-nodes I and J in the global coordinate system.

Node K defines a plane (with I and J) containing the element s-axis.

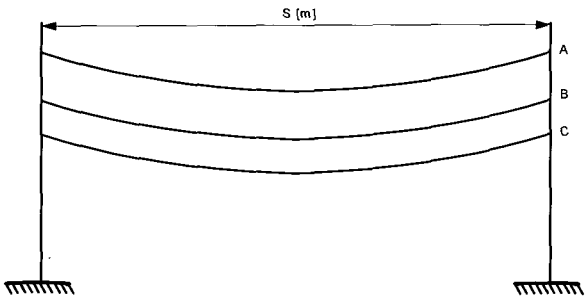

Fig. 5 Three phases without spaces, Case 1.

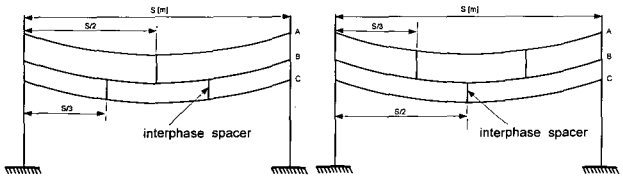

Case 2 Case 3

Fig. 6 Three phases with spaces, Case 2 - Case 3.

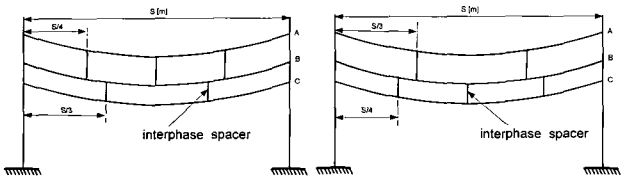

Case 4 Case 5

Fig. 7 Three phases with spaces, Case 4 - Case 5.

This element supports all nonlinear features allowing for explicit dynamic analysis. Belytschko beam with section integration is also applied as a trapezoidal section or two beam-model. The iced conductor presented in Fig. 8a is modeled by two beam-element faces that are connected by the spot weld. In this paper, the iced conductor is modeled by a beam-element (trapezoidal section) in Fig. 8b. The inter-phase spacers also are used by Belytschko beam (rigid body rotations).

By considering an implicit analysis, we obtain the resonance frequency as 4.22 $[rad/s]$. Explicit dynamic analysis is than additionally applied. In this simulation, the wind velocity is $25 \sin \omega t$.

The maximal galloping amplitudes at center of span in Case 1 (without spacer), in time 150 $[s]$ are:

$Uz = 2.34$ $[m]$, $Uz = 1.78$ $[m]$ & $ROTx = 0.97$ $[rad]$.

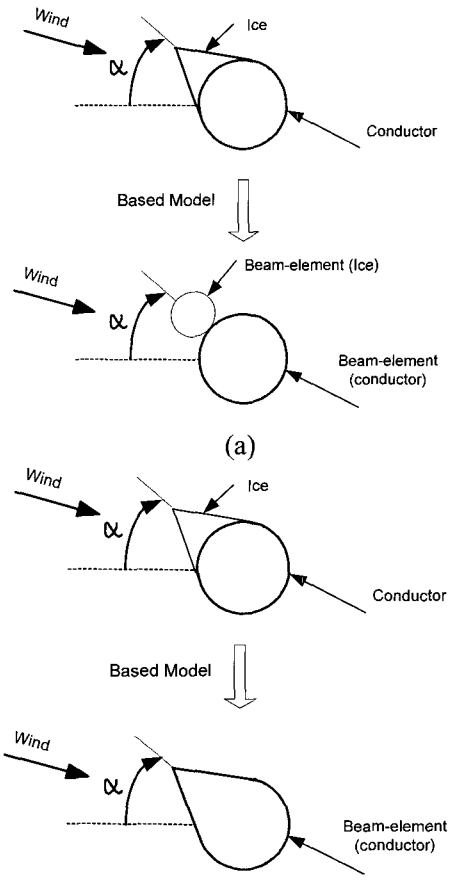

Fig. 8 Section of iced conductor.

Figs. 9-17 and Table 3 show the horizontal Uz vertical Uy, and rotation on x axis $[ROTx]$ in 5 cases, phases: A, B, C.

The results of the computation prove that the amplitude of conductor galloping is reduced by using inter-phase spacers.

5. Conclusion

The main purpose of this paper is to calculate the behaviors of inter-phase spacers to reduce the amplitude

of galloping in conductors. In simulation, three phases and iced single two bundle conductors with/without spacers are considered in viewpoint of standard cases. The implicit/explicit finite element methods are used to calculate the transient response with geometric nonlinear behavior. The ANSYS/LS-DYNA program is also applied. The calculation results may be used to predict the positions to insert the inter-phase spacers between conductors.

Table 3 The amplitude at center of span (Min&Max)

Case		Displ. UZ [m]		Displ. UY [m]		Rotation ROTX[rad]	
		(T1)	(T2)	(T1)	(T2)	(T1)	(T2)
1	A	-2.6 2.3	-1.5 1.3	-0.8 1.7	-0.2 0.7	-0.9 0.9	-0.3 0.2
	B	-2.6 2.3	-1.5 1.3	-0.8 1.7	-0.2 0.7	-0.9 0.9	-0.3 0.2
	C	-2.6 2.3	-1.5 1.3	-0.8 1.7	-0.2 0.7	-0.9 0.9	-0.3 0.2
2	A	-1.6 1.7	-1.4 1.3	-0.1 0.9	-0.2 0.6	-0.2 0.2	-0.2 0.2
	B	-1.3 1.3	-1.2 1.3	-0.1 0.9	-0.1 0.6	-0.2 0.2	-0.2 0.2
	C	-2.2 2.3	-1.2 1.3	-0.5 1.7	-0.3 1.0	-2.3 2.2	-0.4 0.3
3	A	-2.3 2.3	-1.3 1.3	-0.8 1.3	-0.3 0.6	-2.6 2.5	-0.4 0.3
	B	-1.2 1.3	-1.2 1.2	-0.1 0.9	-0.1 0.6	-0.2 0.2	-0.1 0.2
	C	-1.7 1.8	-1.2 1.4	-0.1 1.0	-0.1 0.61	-0.3 0.2	-0.1 0.1
4	A	-1.4 1.4	-1.2 1.3	-0.1 0.7	-0.2 0.6	-0.2 0.2	-0.2 0.2
	B	-1.1 1.3	-1.2 1.3	-0.2 0.8	-0.1 0.6	-0.2 0.2	-0.2 0.2
	C	-2.1 2.3	-1.3 1.3	-0.7 1.6	-0.2 0.9	-1.1 1.1	-0.1 0.1
	A	-1.9 2.3	-1.3 1.1	-0.7 1.5	-0.3 0.8	-0.9 0.9	-0.4 0.3
	B	-1.2 1.3	-1.2 1.3	-0.1 0.7	-0.1 0.1	-0.2 0.2	-0.2 0.2
	C	-1.2 1.3	-1.2 1.3	-0.1 0.7	-0.1 0.6	-0.2 0.2	-0.1 0.1

Notes: Displ. - Displacement
(T1) - Single conductors
(T2) - Two-bundles conductors

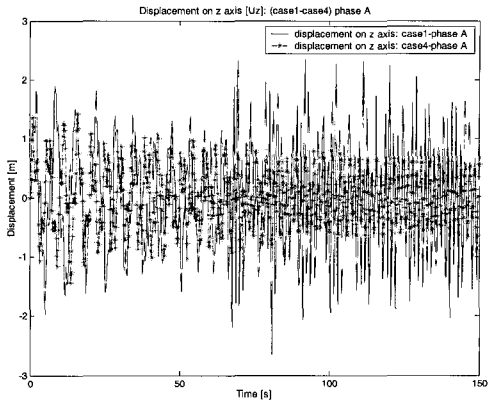

Fig. 9 Displacement on z axis, Case 1-Case 4, Phase A.

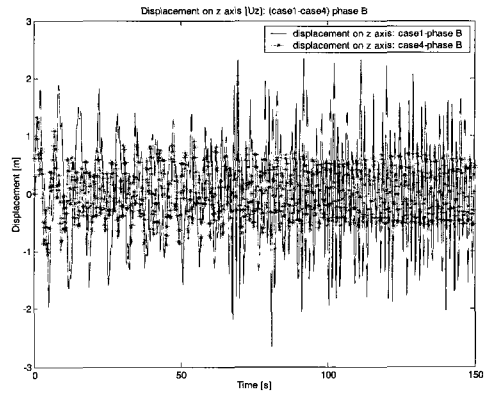

Fig. 10 Displacement on z axis, Case 1-Case 4, Phase B.

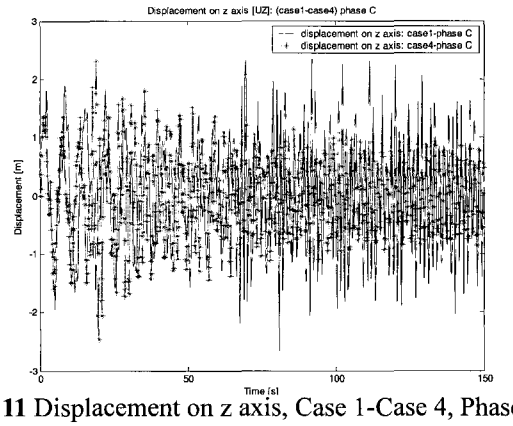

Fig. 11 Displacement on z axis, Case 1-Case 4, Phase C.

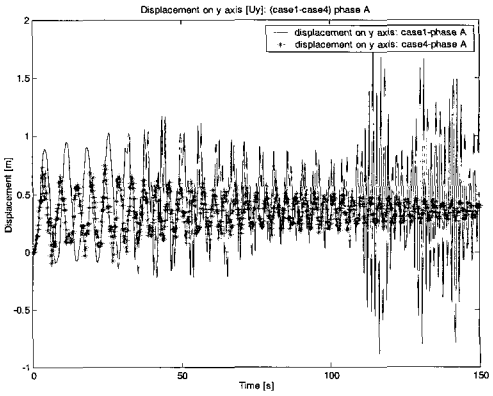

Fig. 12 Displacement on y axis, Case 1-Case 4, Phase A.

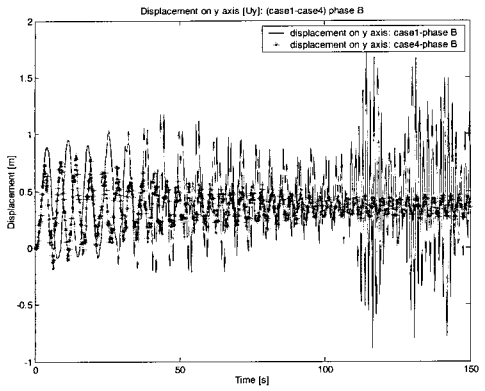

Fig. 13 Displacement on y axis, Case 1-Case 4, Phase B.

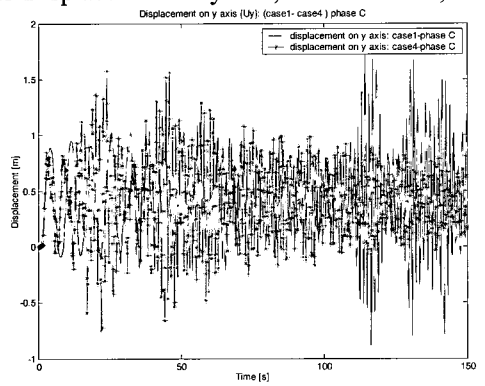

Fig. 14 Displacement on y axis, Case 1-Case 4, Phase C.

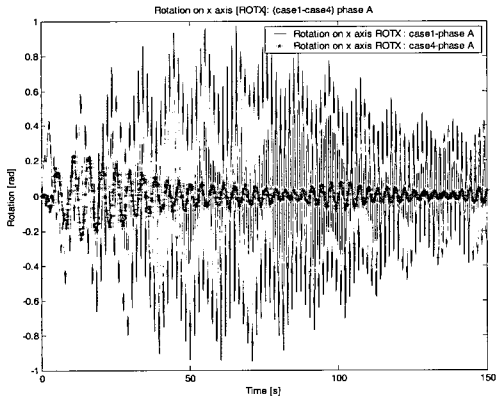

Fig. 15 Rotation on x axis, Case 1-Case 4, Phase A.

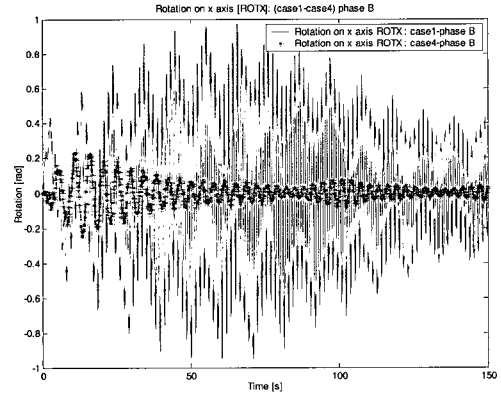

Fig. 16 Rotation on x axis, Case 1-Case 4, Phase B.

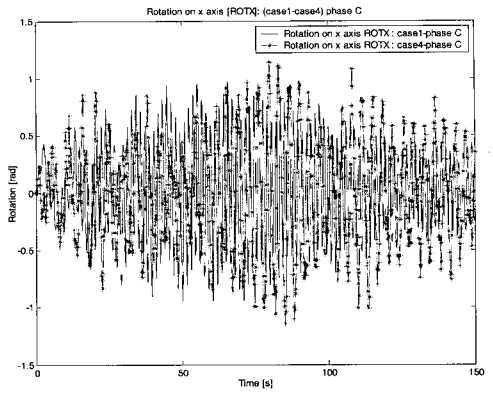

Fig. 17 Rotation on x axis, Case 1-Case 4, Phase C.

References

[1] J.P.Den Hartog, "Transmission line vibration due to sleet," *AIEE Journal*, Vol., 51, 1932.

[2] E.Simiu, R.H. Scanlan, "Wind effects on structures fundamentals and application to design", Wiley and Sons, 1996.

[3] C.J. Noh, H.S. Park and G.S. Byun, "The analysis of power line galloping by describing function method', *The Korean Institute of Electrical Engineers*, Vol. 41, No. 4, pp. 339-345, 1992.

[4] H.S. Kim and G.S. Byun "A study on the analysis of galloping for power transmission line", *ISIE, Pusan, Korea*, pp. 973-978, 2001.

[5] R. Keutgen and J.L. Lilien, "Benchmark cases for galloping with results obtained from wind tunnel facilities-validation of a finite element model", *IEEE.* Vol. 15, No. 1, 2000.

[6] Liming Wang, Yu Yin, Xidong Liang, Zhicheng Guan, "Study on air insulator strength under conductor galloping condition by phase to phase", Annual report conference on Electrical Insulation and Dielectric Phenomena, Department of Electrical, Tsinghua University, China, pp. 617-619, 2001.

[7] H. S. Kim, T. L. Nguyen and G. S. Byun, "A coupled-field analysis of galloping for power transmission line", *ICCAS 2002, International Conference on Control, Automation and Systems*, Jeonbuk, Korea, 2002.

[8] H.S.Kim, T.L.Nguyen, G.S.Byun "Behaviors of spacers on the galloping of power transmission lines," in *Proceedings of the ICCAS Conference*, 2003.

[9] J.O. Hallquist, "LS-DYNA theoretical manual", Livermore Software Technology Corporation, May 1988.

[10] T. Belytschko, and B.J. Hsieh "Nonlinear transient finite element analysis with convected coordinates", *International Journal for Numerical Methods in*

Engineering, No. 7, pp. 255-271, 1973.
[11] T. Belytschko, L.E. Schwer and M.J. Klein "Large displacement, transient analysis of space frames", International Journal for Numerical Methods in Engineering, Vol. 11, No. 1, pp. 65-84, 1977.
[12] T.Belytschko, W. K. Liu, B.Moran, "Nonlinear finite elements for continua and structures", John Wiley & Sons, LTD, 2001.
[13] Grimes, R. G. Lewis, J. G., Simon, H. D., "A shifted block Lanczos algorithm for solving sparse symmetric generalized eigenproblems", SIAM J. Matrix Anal. Appl, Vol. 15, pp. 1- 45, 1994.
[14] Doocy, E. S., A. R., Hard, "Transmission line reference book", Electric Power Research Institute, Palo Alto, California, 1979.

Hwan-Seong Kim
He received his Ph. D. degree from Kumamoto University, Japan in 1996. He is now an Associate Professor with the Department of Logistics, Korea Maritime Univ., Korea. His research interests are in the areas of observer, fault detection and isolation, and supervision of industrial processes.

Tuong-Long Nguyen
He received his Ph. D. degree from Korea Maritime University, Korea in 2005. He is now a Lecturer with the Department of Engineering Mechanics, Faculty of Applied Science, Ho-Chi-Minh City University of Technology, Vietnam.
His research interests are in the areas of dynamical behaviors on structure, fluid-solid interaction analysis, finite element method and system identification.